

## Do surfaces with mixed hydrophilic and hydrophobic areas enhance pool boiling?

Amy Rachel Betz,<sup>1</sup> Jie Xu,<sup>2</sup> Huihe Qiu,<sup>3</sup> and Daniel Attinger<sup>1,a)</sup>

<sup>1</sup>Mechanical Engineering, Columbia University, New York 10027, USA

<sup>2</sup>Mechanical Engineering, Washington State University, Vancouver, Washington 98686, USA

<sup>3</sup>Department of Mechanical Engineering, Hong Kong University of Science and Technology, Clear Water Bay, Kowloon, Hong Kong

(Received 1 August 2010; accepted 6 August 2010; published online 6 October 2010)

We demonstrate that smooth and flat surfaces combining hydrophilic and hydrophobic patterns improve pool boiling performance. Compared to a hydrophilic surface with 7° wetting angle, the measured critical heat flux and heat transfer coefficients of the enhanced surfaces are, up to respectively, 65% and 100% higher. Different networks combining hydrophilic and hydrophobic regions are characterized. While all tested networks enhance the heat transfer coefficient, large enhancements of critical heat flux are typically found for hydrophilic networks featuring hydrophobic islands. Hydrophilic networks indeed are shown to prevent the formation of an insulating vapor layer. © 2010 American Institute of Physics. [doi:10.1063/1.3485057]

Boiling is an efficient process to transfer large amounts of heat at a prescribed temperature because of the large latent heat of vaporization. The term *flow* boiling describes the boiling of liquids forced to move along hot surfaces, while in *pool* boiling, the topic handled in this paper, the liquid is stagnant and in contact with a hot solid surface.<sup>1</sup> Besides the common experience of boiling water in an electric kettle, pool boiling has applications in metallurgy, high performance heat exchangers, and immersion cooling of electronics. Pool boiling performance is measured with two parameters, the heat transfer coefficient (HTC) and the critical heat flux (CHF). The CHF is measured by increasing the surface temperature until a transition from high HTC to very low HTC occurs. This signifies the formation of a vapor film insulating the liquid from the heated surface, a phenomenon called dry out. Several characteristics determine the performance of a boiling surface. Nucleation sites in appropriate number and dimensions need to be provided such as cavities, rough areas, or hydrophobic islands.<sup>2</sup> As of today, the performance of boiling surfaces has been increased by using wicking structures to prevent dry out,<sup>3</sup> by increasing the surface area with fins or fluidized bed,<sup>3-6</sup> and by enhancing the wettability of the surface.<sup>5-10</sup> The latter strategy is justified by experiments of Wang and Dhir,<sup>11</sup> showing that the CHF was increased by enhancing surface wettability. Significant heat transfer enhancement has also been obtained with surfaces coated with a micrometer thick carpet of nanometer diameter rods (nanorods).<sup>5-7</sup> The CHF enhancement was attributed to coupled effects such as the multiscale geometry<sup>5,7</sup> and the superhydrophilicity of the nanowire arrays.<sup>6,7</sup>

A common assumption<sup>1</sup> in boiling studies is that the surface has a unique value of wettability. However, the above introduction shows that the influence of wettability on boiling is complex: while hydrophobic zones promotes nucleation, the surface hydrophilicity does enhance the CHF.<sup>9</sup> In this work we micro-manufacture surfaces combining hydrophobic and hydrophilic zones, for pool boiling experiments. Our intuition is that a well-designed network of hy-

drophobic and hydrophilic regions might promote nucleation, enhance the HTC, and increase the CHF by preventing dry out.

Hydrophobic and hydrophilic regions were manufactured on oxidized silicon wafers as shown in Fig. 1. The hexagonal pattern size  $d$  was typically between 40% and 60% of the pitch  $p$  between patterns. We varied  $p$  from 50 to 200  $\mu\text{m}$ , as well as the connectivity of the hydrophobic and hydrophilic patterns. Hydrophilic surfaces with hydrophobic islands were called *hydrophilic networks*, and noted (+), meaning that any two hydrophilic regions could be joined without passing over a hydrophobic zone. Hydrophobic surfaces with hydrophilic islands were called *hydrophobic networks*, and noted (-). The hydrophobic coating of Teflon (AF400, Dupont) was patterned using standard photolithography techniques. On the bottom side of the wafer, we deposited an Indium Tin Oxide (ITO) heater with Copper electrodes and a 100 nm SiO<sub>2</sub> passivation layer. A thin thermocouple (Omega CO2, K-type) was taped onto the center of the ITO heater using a polyimide adhesive pad. A 5 mm thick polydimethylsiloxane layer was then used to seal and insulate the bottom side of the wafer. Optionally, a final step was added to increase the wettability, by rinsing the top side of the wafers for a few seconds with a diluted solution of buffered hydrofluoric acid (HF). The wettability was measured to be 110° for the Teflon, 10°–25° for the SiO<sub>2</sub> and 7° for the SiO<sub>2</sub> treated with HF. The maximum height of the hydrophobic patterns was 100 nm, while the roughness was below 5 nm. No difference in pattern height was observed

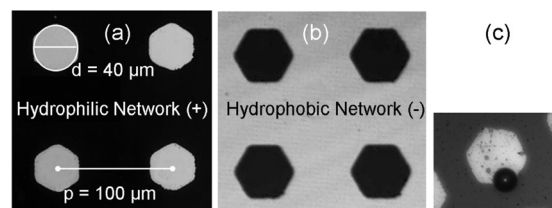


FIG. 1. Typical micrographs (a) and (b) of surfaces with hydrophilic (black) and hydrophobic (gray) zones. The pattern diameter  $d$  is the diameter of the inscribed disk. The pattern pitch is  $p$ . At low superheat, bubbles typically nucleate at the interface between areas of different wettability (c).

<sup>a)</sup>Author to whom correspondence should be addressed. Electronic mail: da2203@columbia.edu.

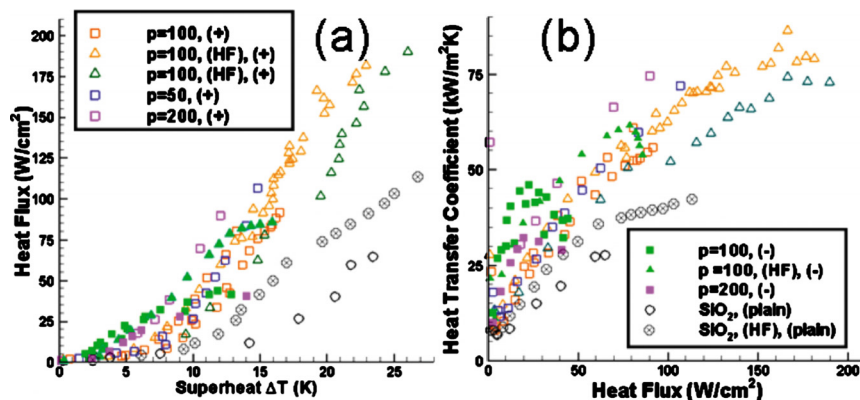


FIG. 2. (Color online) Pool boiling curves with heat flux as a function of the superheat (a) and heat transfer coefficient as a function of heat flux (b), for patterned and plain wafers. Legend shows pitch  $p$  in  $\mu\text{m}$ , use of an optional HF treatment and the type of network (see Fig. 1). The maximum uncertainty on the heat flux was estimated as  $\pm 1.5 \text{ W/cm}^2$ , caused by the measurement of the heater area and the electrical power. The maximum uncertainty on the superheat was estimated as  $\pm 1.5 \text{ K}$ , due to the thermocouple, temperature acquisition and heater/wafer thickness measurement uncertainties. For superheat values larger than 1 K the uncertainty on the heat transfer coefficient is typically less than  $3 \text{ kW/m}^2\text{K}$ .

after the HF treatment. More details on the manufacturing process are provided in the supplementary document.<sup>12</sup>

Heat transfer measurements are run using a pool boiling setup similar to the one in Ref. 6. The wafer is placed in a polycarbonate chamber open to the atmosphere, filled with degassed, deionized water. The water is maintained at the saturation temperature of  $100 \text{ }^\circ\text{C}$  by immersed 100W cartridge heaters. A 750 W power supply (Agilent N5750A) applies a given heat flux to the  $1 \text{ cm}^2$  ITO heater. A data acquisition system (OMEGA DAQ-55) is used to record the temperature measured on the back of the wafer,  $T_{\text{meas}}$ . The temperature at the wafer-water interface  $T_w = T_{\text{meas}} - q''t/k$  is then determined using Fourier's law, with  $q''$ ,  $t$ , and  $k$  the respective heat flux, wafer thickness and silicon thermal conductivity. For each data point presented in Fig. 2, the temperature is obtained by averaging 300 readings over about three minutes. The CHF is determined as the heat flux corresponding to the last observed stable temperature, beyond which a sudden dramatic increase in temperature is observed.

Measurements of boiling performance are shown in Fig. 2, which compares the plain SiO<sub>2</sub> surfaces to surfaces featuring hydrophobic or hydrophilic networks. Figure 2(a) shows the typical heat flux  $q''$  versus superheat  $\Delta T = T_w - T_{\text{sat}}$  curve. Values of CHF for a plain wafer treated with HF are about  $115 \text{ W/cm}^2$  at  $\Delta T = 27 \text{ K}$ , consistent with the  $110 \text{ W/cm}^2$  at  $\Delta T = 33 \text{ K}$  obtained in Ref. 8 for a surface with slightly larger ( $14^\circ$ ) wetting angle, shown in Fig. 3. All patterned

surfaces exhibit a boiling curve steeper than the plain wafers, with values of CHF ranging from 90 to  $190 \text{ W/cm}^2$ , up to 165% of the values of the plain wafer. The highest CHF was reached for a pitch of  $100 \mu\text{m}$ . Patterned surfaces treated with HF exhibit a much higher CHF than untreated patterned surfaces. In the three tested instances, hydrophobic networks exhibit a significantly lower CHF than the hydrophilic networks, sometimes even lower than plain SiO<sub>2</sub> surfaces. Figure 2(b) shows the HTC as a function of the heat flux. For heat fluxes lower than  $50 \text{ W/cm}^2$ , three groups of surfaces can be distinguished by their HTC. Plain surfaces exhibit the lowest HTC, hydrophilic networks show intermediate HTC values, and hydrophobic networks show the maximum HTC values. For heat fluxes higher than  $50 \text{ W/cm}^2$ , the HTC of the hydrophilic networks increases to values up to  $85 \text{ kW/m}^2\text{K}$ , which is twice the max HTC of the plain SiO<sub>2</sub> surfaces. As a summary, patterning of mixed hydrophilic and hydrophobic areas can improve the CHF and HTC of a plain hydrophilic surface by 65% and 100%, respectively. While surfaces with hydrophilic networks enhance both the CHF and HTC, surfaces with hydrophobic networks seem to only enhance the HTC and might even reduce the CHF. As shown by the comparison in Fig. 3, the maximum values obtained in this work are comparable to the maximum HTC and CHF obtained on surfaces covered with a carpet of nanowires<sup>5,6</sup> but slightly lower than sintered wicking surfaces such as in Ref. 3. The surfaces studied in this work however are planar while the surface in Refs. 3, 5, and 6 can be considered as extended surfaces which promote wicking transport. Since the enhanced surfaces have more than a unique wetting angle value they are represented by horizontal lines in Fig. 3.

Explaining the observed trends is challenging because pool boiling is a transient, multiphase phenomenon, visualization is difficult especially for the violent boiling near CHF, and the geometry and wettability of these enhanced surfaces is complex. The following however can be said

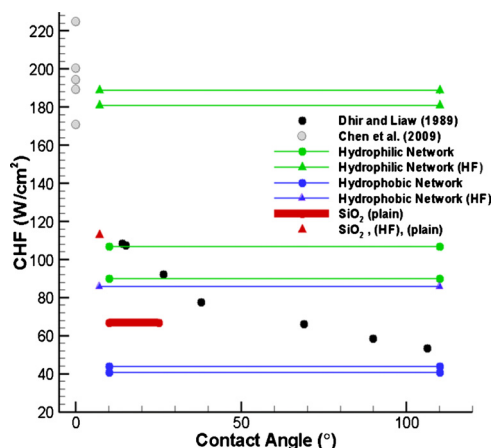


FIG. 3. (Color online) CHF as a function of wetting angle. Our results are in color, with horizontal lines for cases where the surfaces had regions of mixed wettabilities. Black and gray dots are comparison data on respectively surfaces with controlled wetting properties and a superhydrophilic carpet of nanowires.

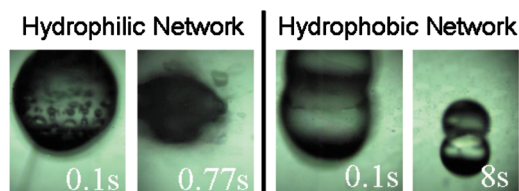


FIG. 4. (Color online) The evaporation of a  $3 \mu\text{l}$  water drop on two patterned surfaces heated at  $132 \text{ }^\circ\text{C}$ , the left surface exhibiting a hydrophilic network and the right surface, a hydrophobic network. For these experiments the patterns are square, with a pitch of  $250 \mu\text{m}$ .

from the theoretical and experimental body of literature summarized in Refs. 1, 13, and 14. First, the enhancement of HTC on patterned surfaces can be explained by the increased availability of active nucleation sites. Indeed, the nucleate boiling theory of Mikic and Rohsenow,<sup>15</sup> states that  $HTC=q''/\Delta T$  depends linearly on the density of nucleation sites. Interestingly, experiments in Fig. 1(c) repeatedly show that bubbles start nucleating on the edge hydrophobic patterns. The edges of the lower conductivity patterns also correspond to local maxima of heat flux density, which have been shown to facilitate the onset of nucleate boiling, in experiments with conductive surfaces covered with perforated polymer films.<sup>16</sup> Mikic and Rohsenow's theory might also explain why the HTC of hydrophobic networks is higher than the HTC of hydrophilic networks, since hydrophobic networks offer a larger hydrophobic area, therefore more nucleation sites. Second, the patterns might also constrain the distance between the nucleation sites, which can moderate instabilities and enhance the CHF. Indeed, as stated by Zuber,<sup>1,17</sup> the dryout responsible for CHF is caused by Helmholtz instabilities that merge individual bubble columns. On a plain surface the typical pitch  $\lambda$  between the bubble columns is determined by the Taylor instability  $\lambda=2\pi\sqrt{3\sigma/g(\rho_l-\rho_v)}=27\text{ mm}$ <sup>1</sup> where  $\sigma$  is the interfacial tension between water and water vapor and  $\rho_l$  and  $\rho_v$  are their densities, respectively. According to the same theory, the critical vapor velocity that triggers Helmholtz instabilities is inversely proportional to  $\lambda^{-0.5}$ . This analysis concludes to a maximum "practical" CHF value around  $110\text{ W/cm}^2$ . Let us assume now that the regular patterns investigated in this study constrain the wavelength of the instabilities to the pattern pitch  $\lambda_p$ . In that case,  $\lambda_p$  between 200 and  $50\text{ }\mu\text{m}$  would multiply the attainable CHF by  $(\lambda/\lambda_p)^{0.5}$ , a factor between 11 and 23. For hydrophilic networks, the improvement measured experimentally is "only" 1.65, which indicates that other limiting factor might come into play.<sup>18</sup> Third, the observed influence of the HF treatment in increasing CHF (but not HTC) can be explained by the wettability increase in the hydrophilic regions<sup>8</sup> or by the increased difference in wettability between the hydrophobic and hydrophilic regions. Fourth, the fact that hydrophilic networks show a large CHF enhancement, while hydrophobic networks do not show this CHF enhancement can be explained by the droplet boiling experiments in Fig. 4, recorded with a high-speed camera. A  $3\text{ }\mu\text{L}$  water droplet is gently deposited on two patterned surface heated to an initial temperature of  $132\text{ }^\circ\text{C}$ , a hydrophilic network on the left, versus a hydrophobic network on the right. At 0.1 s on the hydrophilic network, several individual bubbles have nucleated. A very dynamic boiling process occurs then, visible from the strong and fast perturbations on the drop free surface ( $t=0.77\text{ s}$ ). Despite the strong boiling, the drop does not move significantly, being held to the substrate. On the hydrophobic network, the drop shows a different behavior: at  $t=0.1\text{ s}$ , the drop does not seem to wet the substrate, as evidenced by the circular shadow under the

drop. No individual bubbles are visible, and the drop moves toward the bottom right of the field of view during the evaporation. The total evaporation times of 11 s is one order of magnitude larger than the evaporation time on the hydrophilic network. The sliding, absence of individual bubbles, and larger evaporation time suggest the presence of an insulating vapor film between the drop and the substrate, analog to the Leidenfrost phenomenon. While the transient experiments in Fig. 4 are not equivalent to steady state pool boiling experiments, they suggest that hydrophilic networks help nucleation and enhance CHF by preventing the early formation of a vapor film, while hydrophobic networks, where vapor bubbles can easily merge, favor early occurrence of CHF. Indeed the hydrophobic networks, unless treated with HF, exhibit a lower CHF than the bare  $\text{SiO}_2$ , probably because they promote the formation of a vapor film. As a final observation, we note that the size of the patterns is compatible with the size of the active nucleation sites predicted by Hsu's theory.<sup>19</sup> A detailed analysis of the nucleation site size can be found in the supplementary document.<sup>12</sup>

In summary, we have demonstrated that surfaces with networks combining hydrophilic and hydrophobic regions significantly enhance the CHF and the HTC during pool boiling. The best enhancement arises with hydrophilic networks featuring hydrophobic islands, which efficiently prevent the formation of an insulating vapor layer.

D.A. is grateful for the help of NSF CAREER Grant No. 0449269, which allowed for his 2008 visit to the Hong Kong laboratory of H.Q. to start this project.

<sup>1</sup>V. Carey, *Liquid-Vapor Phase Change Phenomena* (Taylor & Francis, London, 1992).

<sup>2</sup>Y. Nam and Y. S. Ju, *Appl. Phys. Lett.* **93**, 103115 (2008).

<sup>3</sup>J. A. Weibel, S. V. Garimella, and M. T. North, *Int. J. Heat Mass Transfer* **53**, 4204, (2010).

<sup>4</sup>L. H. Chien and R. L. Webb, *Exp. Therm. Fluid Sci.* **16**, 332 (1998).

<sup>5</sup>C. Li, Z. Wang, P. I. Wang, Y. Peles, N. Koratkar, and G. P. Peterson, *Small* **4**, 1084 (2008).

<sup>6</sup>R. Chen, M.-C. Lu, V. Srinivasan, Z. Wang, H. H. Cho, and A. Majumdar, *Nano Lett.* **9**, 548 (2009).

<sup>7</sup>S. Kim, H. D. Kim, H. Kim, H. S. Ahn, H. Jo, J. Kim, and M. H. Kim, *Exp. Therm. Fluid Sci.* **34**, 487 (2010).

<sup>8</sup>V. K. Dhir and S. P. Liaw, *J. Heat Transfer* **111**, 739 (1989).

<sup>9</sup>C. H. Wang and V. K. Dhir, *J. Heat Transfer* **115**, 670 (1993).

<sup>10</sup>B. J. Jones, J. P. McHale, and S. V. Garimella, *J. Heat Transfer* **131**, 121009, (2009).

<sup>11</sup>C. H. Wang and V. K. Dhir, *J. Heat Transfer* **115**, 659 (1993).

<sup>12</sup>See supplementary material at E-APPLAB-97-061035 for details on microfabrication and nucleation site size.

<sup>13</sup>V. K. Dhir, *Annu. Rev. Fluid Mech.* **30**, 365 (1998).

<sup>14</sup>I. L. Pioro, W. Rohsenow, and S. S. Doerffer, *Int. J. Heat Mass Transfer* **47**, 5033 (2004).

<sup>15</sup>B. B. Mikic and W. M. Rohsenow, *J. Heat Transfer* **91**, 245 (1969).

<sup>16</sup>V. A. Antonenko, *J. Eng. Phys. Thermophys.* **54**, 391 (1988).

<sup>17</sup>N. Zuber, Ph.D. thesis, UCLA, Los Angeles, CA, 1959.

<sup>18</sup>R. W. Schrage, *A theoretical Study of Interphase Mass Transfer* (Columbia University Press, New York, NY, 1953).

<sup>19</sup>Y. Y. Hsu *J. Heat Transfer* **84**, 207 (1962).